JOURNAL OF CHEMICAL INFORMATION AND MODELING

Article

pubs.acs.org/jcim

# Novel Mycosin Protease $MycP_1$ Inhibitors Identified by Virtual Screening and 4D Fingerprints

Adel Hamza,[‡,†] Jonathan M. Wagner,[†,‡] Timothy J. Evans,[†,‡] Mykhaylo S. Frasinyuk,[†,∥,⊥] Stefan Kwiatkowski,[†,∥] Chang-Guo Zhan,[§,∥] David S. Watt,[†,§,∥] and Konstantin V. Korotkov*[,†,‡]

[†]Department of Molecular and Cellular Biochemistry, University of Kentucky, Lexington, Kentucky 40536, United States

[‡]Center for Structural Biology, University of Kentucky, Lexington, Kentucky 40536, United States

[§]Department of Pharmaceutical Sciences, College of Pharmacy, University of Kentucky, Lexington, Kentucky 40536, United States

[∥]Center for Pharmaceutical Research and Innovation, University of Kentucky, Lexington, Kentucky 40536, United States

[⊥]Institute of Bioorganic Chemistry and Petrochemistry, Kyiv-94, 02660, Ukraine

Supporting Information

**ABSTRACT:** The rise of drug-resistant *Mycobacterium tuberculosis* lends urgency to the need for new drugs for the treatment of tuberculosis (TB). The identification of a serine protease, mycosin protease-1 ($MycP_1$), as the crucial agent in hydrolyzing the virulence factor, ESX-secretion-associated protein B (EspB), potentially opens the door to new tuberculosis treatment options. Using the crystal structure of mycobacterial $MycP_1$ in the apo form, we performed an iterative ligand- and structure-based virtual screening (VS) strategy to identify novel, nonpeptide, small-molecule inhibitors against $MycP_1$ protease. Screening of ∼485 000 ligands from databases at the Genomics Research Institute (GRI) at the University of Cincinnati and the National Cancer Institute (NCI) using our VS approach, which integrated a pharmacophore model and consensus molecular shape patterns of active ligands (4D fingerprints), identified 81 putative inhibitors, and *in vitro* testing subsequently confirmed two of them as active inhibitors. Thereafter, the lead structures of each VS round were used to generate a new 4D fingerprint that enabled virtual rescreening of the chemical libraries. Finally, the iterative process identified a number of diverse scaffolds as lead compounds that were tested and found to have micromolar $IC_{50}$ values against the $MycP_1$ target. This study validated the efficiency of the SABRE 4D fingerprints as a means of identifying novel lead compounds in each screening round of the databases. Together, these results underscored the value of using a combination of *in silico* iterative ligand- and structure-based virtual screening of chemical libraries with experimental validation for the identification of promising structural scaffolds, such as the $MycP_1$ inhibitors.

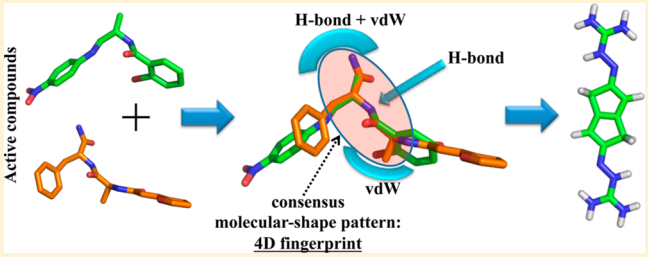


## INTRODUCTION

*Mycobacterium tuberculosis*, the agent causing tuberculosis (TB), is responsible for significant worldwide morbidity and mortality, estimated at more than 1.3 million deaths in 2012 according to the World Health Organization.[1] This ancient but persistent disease still lacks effective antimicrobial treatment regimens, particularly in cases of multidrug-resistant tuberculosis.[2,3] An attractive target for development of new antimicrobials is the recently identified mycobacterial protein-export machinery.[4−6] *M. tuberculosis* relies on specialized ESX secretion systems, also called Type VII Secretion (T7S) Systems, to evade the human immune system and promote bacterial survival within host cells,[7,8] and it possesses five gene clusters that encode sets of conserved proteins comprising the ESX systems.[9] Each of these gene clusters, called ESX-1 through ESX-5, includes essential mycosin proteases, which are named $MycP_1$ through $MycP_5$, respectively.

The mycosins are membrane-bound serine proteases belonging to the subtilisin family of proteases.[10,11] The crystal structures of $MycP_1$ and $MycP_3$ revealed that these mycosins are characterized by a relatively deep, broad, substrate-binding groove and by the absence of an autoinhibitory propeptide, making them the first subtilisins that do not undergo post-translational processing.[12−14] $MycP_1$ is known to hydrolyze the important virulence factor ESX secretion-associated protein B (EspB).[15−17] $MycP_1$ cleaves the unstructured C-terminal part of EspB, possibly activating EspB for phospholipid binding.[18] Most importantly, inactivation of $MycP_1$ leads to decreased virulence of *M. tuberculosis* and increased survival in the mouse model of TB.[17] These data, combined with the availability of $MycP_1$ crystallographic structures, make $MycP_1$ an attractive target for development of antimicrobial compounds for the treatment of TB.[19,20] The structural characteristics of the $MycP_1$ substrate-binding pocket differ substantially from known subtilisins whose structures were solved with bound inhib-

**Received:** January 13, 2014
**Published:** March 16, 2014

  

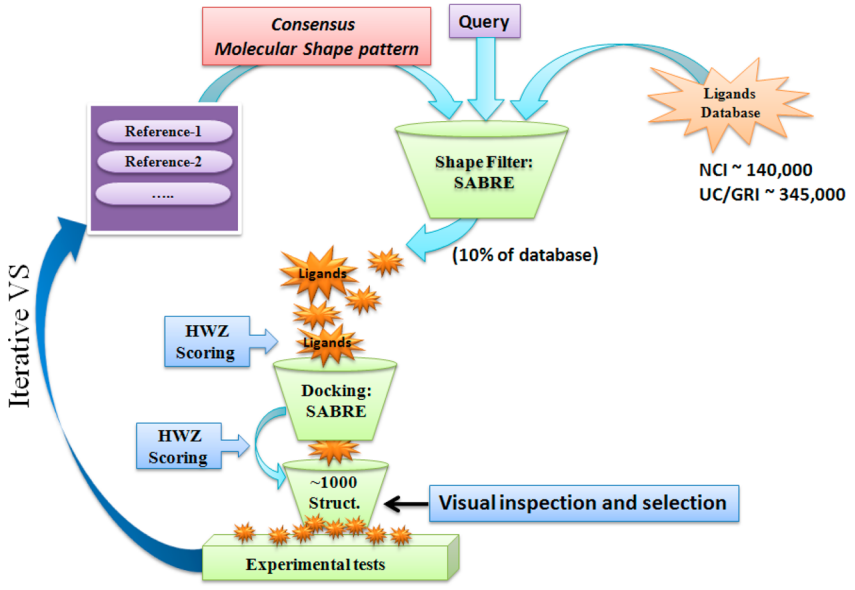


**Figure 1.** Flowchart of the VS process.

itors,[21] and the commercially available subtilisin inhibitors and protease inhibitor cocktails displayed little or no inhibition of $MycP_1$ (Supporting Information Table 1).

*In vitro* High Throughput Screening (HTS) in conjunction with *in silico* virtual screening represent complementary methods for the identification of $MycP_1$ inhibitors. Although HTS alone has been used successfully to identify new leads in drug discovery, it remains a costly and time-consuming process. Various computational approaches are available at present to complement HTS technologies, including the popular, virtual screening (VS) techniques.[22−25] VS consists of approaches that either take the structure of the target protein into account (structure-based screening) or rely solely on structures of known bioactive molecules (ligand-based screening). The ligand- and structure-based VS strategies are not mutually exclusive and are often used in parallel. We and others have reported the successful application of these VS methods for lead structure identification,[26−29] and many VS software packages are available,[30−32] as summarized by Reddy.[33] Although the algorithms for these VS methods exploit different types of structural "fingerprints" and scoring functions, their performance varies significantly depending on the specific targets.[34−36]

As part of an integrated, reiterative program of virtual *in silico* lead identification, *in vitro* screening, and laboratory synthesis, we developed two approaches that enhance the effectiveness of the combined ligand- and structure-based VS and hold promise for the development of new classes of $MycP_1$ inhibitors. Previously, we reported an efficient 3D shape-based similarity algorithm including an effective 3D shape-fitting procedure and a robust scoring function (HWZ score).[37] We also improved the VS algorithm using an enhanced molecular shape-density model called Shape Approach Based Routines Enhanced (SABRE),[37] and we applied this algorithm to a number of medically relevant proteins.[38−42] SABRE is unique in that it takes advantage of the structural features of known ligands to generate a consensus molecular-shape pattern (*i.e.*, a "4D fingerprint") that filters out unacceptable candidates and identifies desired candidates that fit in the binding pocket. The successful performance of SABRE[37,43,44] in ranking screened compounds for the 40 databases of the Directory of Useful Decoys (DUD) prompted us to apply this method to the challenging $MycP_1$ target for which no inhibitors have been thus far reported.

We now report the successful application of this ligand- and structure-based virtual screening approach in the discovery of inhibitors that target the active site of the $MycP_1$ protease. Four compounds were identified by SABRE that showed inhibitory activity against $MycP_1$ with $IC_{50}$ values in the micromolar range and that provide diverse scaffolds as starting points for the development of small-molecule antagonists of $MycP_1$. This study further validated the SABRE 4D fingerprint algorithm as a means of identifying potential inhibitors and providing departure points for laboratory synthesis.

## METHODS

To identify potential inhibitors of $MycP_1$ protease, we employed VS, according to the flowchart in Figure 1, using a merged compound library from GRI and the NCI downloaded from the ZINC database.[45] The structure-based VS (docking) study utilized the recently reported X-ray structure of *M. thermoresistibile* $MycP_1$ protease (PDB ID: 4HVL).[12] We generated multiple conformations of each ligand in the database using OMEGA (OpenEye Scientific Software).[46−48] Atom typing, energy calculations, and geometry optimization in OMEGA were performed using the Merck Molecular Force Field (MMFF). The maximum allowed number of conformations per compound was 200, and the energy window, which was the value used to discard high-energy conformations, was set at 10 kcal/mol.

**Ligand Shape-Based Virtual Screening.** The ligand 3D-shape-based similarity method of SABRE was used as the first filter in the VS strategy.[37,43,44] Briefly, the shape-based VS method takes into account both the structural diversity of each ligand and the HWZ scoring function. Thus, the superimposition of molecules A and B is scored according to the shape-density overlap $V_{AB}$ between the query (molecule A) with shape-density $V_A$ and testing structure (B) with shape-density $V_B$. Subsequently, the ligands are ranked according to a


dx.doi.org/10.1021/ci500025r | J. Chem. Inf. Model. 2014, 54, 1166−1173

uniform scoring function, denoted by Hamza–Wei–Zhan (HWZ) score for convenience.[37]

$$\mathrm{HWZ} = \sum_{k=1}^{N}\left[a_k\left(\frac{V_{AB}}{V_A}\right)^k + b_k\left(\frac{V_{AB}}{V_B}\right)^k + c_k\left(\frac{V_{AB}}{V_A + V_B}\right)^k\right]$$

The coefficients $a_k$, $b_k$, and $c_k$ have been recalibrated from the previous version.

The VS approach includes two stages: the calculation of the optimal coefficients of the shape-density function using a set of known lead compounds and the utilization of these optimal coefficients during the automated ligand/structure shape-based screening of candidate structures. The active structures are ranked according to how well they complement the shape of the binding site and by the degree of differences in molecular shape between the active ligand and inactive (decoy) molecules. SABRE builds a consensus molecular-shape pattern (*i.e.*, a 4D fingerprint) defined by the coefficients $[c_1, c_2, ....,c_n]$ using a set of active ligands, in which the maximum diversity of pharmacophores is taken into account during the screening of the compound library.[43,44]

Unlike other ligand based shape-overlapping methods,[36,49,50] our approach efficiently detects the key pharmacophore groups of the active ligands responsible for binding to the target. The main improvement in our method lies with consideration of "*virtual*" similar inactive structures (decoys) during the consensus molecular shape pattern detection process. After similarity scoring, the selected structures are further ranked according to the shape complementarity of the receptor-binding site.

In the SABRE algorithm, the shape-density model is enhanced and defined as a linear combination of weighted atomic Gaussian functions.[37] Thus, the molecular shape-density is the sum of all individual weighted pharmacophore densities, and the molecular volume can be rewritten as

$$V = \sum_k C_k V_k^{\mathrm{pharm}}$$

where $V_k^{\mathrm{pharm}}$ is the volume of the pharmacophore $k$.

The optimal coefficients $C_k$ are determined by iteratively adjusting the coefficients using the set of known active ligands $\{A_i\}$ and "*virtual*" decoy structures $\{B_i\}$ (*virtual decoys are chemically possible compounds that are not necessarily synthetically feasible*) until they satisfy these two criteria: for $A \in \{A_i\}$

$$\langle V_A | V_B \rangle = \max \text{ if } B \in \{A_i\} \text{ and } \langle V_A | V_B \rangle = \min \text{ if } B \in \{B_i\}$$

The algorithm builds an efficient *consensus molecular-shape pattern* in which the optimal coefficients $\{C_k\}$ define the *4D fingerprint* of the entire set of active ligands and take into account the structural similarity and chemical features of inactive structures (decoys).[37,44] Therefore, the "4D fingerprint" encodes the (3D) shapes of the known active ligand structures in their multi conformational states (1D).

**Structure Shape-Based Virtual Screening.** The "docking option" available within the SABRE program[37,42,44] placed the filtered conformations of each ligand into the binding cavity of the $MycP_1$ X-ray structure[12] (PDB ID: 4HVL). During this shape-fitting process, the specific conformation was placed into a grid box encompassing all active-site atoms within the receptor-binding site. The volume of the receptor-binding pocket was calculated using a smooth Gaussian function.[44] The docking strategy exhaustively explored all possible positions of each ligand in the binding site and generally focused upon two parameters: shape-fitting and ligand-pose optimization, where ligand-pose is defined as a specific ligand–receptor conformation. The ligand-pose ensemble was then filtered to reject arrangements that did not have sufficient complementarity with the active site of the protein and was next filtered to reject those arrangements lacking significant *van der Waals* contacts with nearby residues. For $MycP_1$ protease, the ligands were filtered based on *van der Waals* contacts with the Ser202, Ala236, S334, and Thr333 side chains. Finally, the screened ligands were ranked using the HWZ scoring function.[37]

**Molecular Modeling of the Binding of the Octapeptide AVKAASLG with $MycP_1$.** We utilized reported procedures for the docking and solvated molecular dynamics (MD) simulations procedures of the $MycP_1$–peptide complex.[27,42] The docking and MD simulations procedures are described in the Supporting Information.

***In Vitro* Assay of $MycP_{1mth}$ Inhibitors.** Recombinant *M. thermoresistibile* $MycP_1$ was expressed and purified as reported previously.[12] In quenched fluorescent peptide assays, $MycP_1$ (1 $\mu$M) was used to digest 20 $\mu$M of a fluorescent peptide substrate, AbzAVKAASLGK(Dnp)OH (GenScript Inc.). Potential $MycP_1$ inhibitors were dissolved in DMSO at 30 mM final concentrations and subsequently diluted with a buffer (50 mM HEPES pH 7.5, 100 mM NaCl) to the desired concentrations. Inhibitors were screened in duplicate in 96-well format at 150 $\mu$M concentrations by adding compounds to $MycP_1$ immediately prior to the addition of the fluorescent peptide. Hydrolysis of the fluorescent peptide was measured by following the increase in fluorescence in a SpectraMaxGemini XPS plate reader (Molecular Devices, LLC) with the following settings: excitation = 319 nm, emission = 419 nm. The initial rate for each inhibitor was calculated using the Softmax Pro software (Molecular Devices, LLC). Inhibitors with high intrinsic fluorescence at time zero were eliminated from further consideration. Rates of the remaining compounds were compared to controls (DMSO-buffer blank) in order to estimate the percent inhibition of individual compounds.

The same *in vitro* assay was utilized to measure $IC_{50}$ of compounds that displayed at least 50% inhibition at 150 $\mu$M concentrations. Inhibitors were added at 0, 5, 10, 50, 100, 200, 350, and 500 $\mu$M concentrations, and DMSO was added such that the final DMSO concentration in each well was the same (2% v/v). Initial rates of fluorescent peptide hydrolysis were measured in triplicate and converted to percentages of baseline activity. Dose–response curves were calculated using the sigmoidal dose–response option in GraphPad Prism version 4.00 (GraphPad Software, Inc.). $IC_{50}$ values were calculated using GraphPad plotted rates of $MycP_1$ activity as a function of log([inhibitor]) and fitted to a sigmoidal curve constrained to 100% activity (*top*) and 0% activity (*bottom*) (Supporting Information Figure 1).

## RESULTS AND DISCUSSION

The $MycP_1$ protease recognized the cleavage site sequence ...–AVKAA$^{358}$|SLG–... within an unstructured portion of EspB.[12,13] Consequently, the $MycP_1$ protease readily processed a fluorescently labeled peptide analogue, AbzAVKAASLGK-(Dnp)OH, that had a $K_m$ of 60 $\mu$M.[12] Molecular docking of the peptide revealed relatively few, low-energy $MycP_1$–peptide complexes. The $MycP_1$–peptide complex that oriented the expected peptide residues in positions P1 and P2, which lie near the catalytic Ser334 side-chain, had the largest number of


dx.doi.org/10.1021/ci500025r | J. Chem. Inf. Model. 2014, 54, 1166–1173

low-energy binding conformations or poses. The docked peptide was further refined by performing MD simulations in which the stability of the MD-simulated $MycP_1$–peptide complex was described by the time dependence of the root-mean-square deviation (RMSD) values of the peptide backbone (Supporting Information Figure 2). The refined $MycP_1$–peptide complex displayed a peptide backbone bound to the catalytic active site of $MycP_1$ through hydrogen bonds with the backbone of the protein (Figure 2). These hydrogen bonds

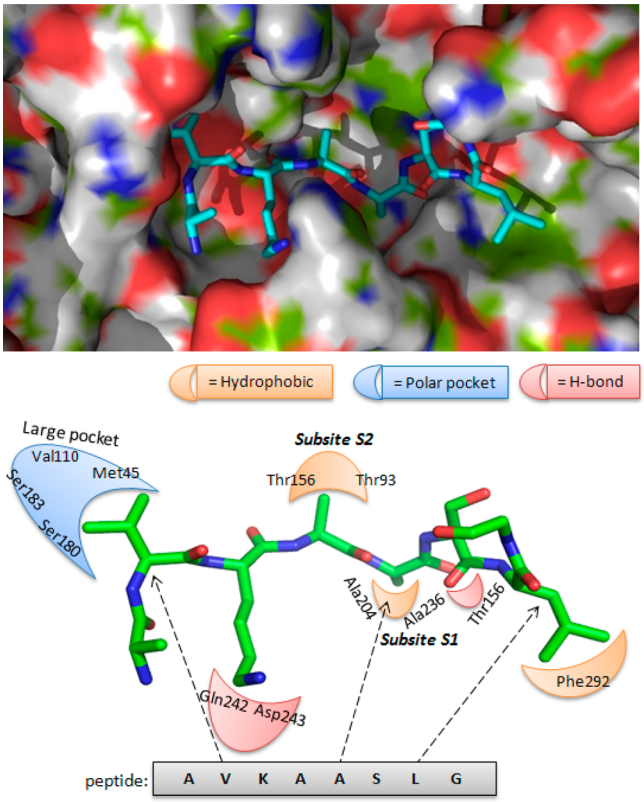


**Figure 2.** (*Top*) Preferred binding conformation of the peptide substrate in the $MycP_1$ active site. (*Bottom*) Pharmacophoric model describing key interactions of the peptide with the $MycP_1$ residues.

included contacts between (H)AVKAASLGK(OH) with Thr333, Ser202, Glu203, and Ala331. In addition, we observed that the Lys side chain of the peptide was stabilized through H-bonding and long-range, electrostatic interactions with the Gln242 and Asp243 side-chains of the $MycP_1$ binding pocket.

Finally, the interactions between the peptide and active site amino acids were analyzed, and pharmacophore features, such as hydrogen bond acceptors and donors, and hydrophobic areas were mapped. Guided by this docking study, we generated a primary topographical interaction model to guide the subsequent VS process (Figure 2). We reasoned that inhibitors that interacted with the $MycP_1$ binding site in a fashion similar to (H)AVKAASLGK(OH) should also compete effectively with EspB in the active site. Because of our prior successes, we utilized the SABRE program for the VS campaign and identified potential inhibitors that occupied the active site of $MycP_1$ (Figure 2) and displayed binding energies comparable or superior to the peptide (H)AVKAASLGK(OH).

In the first stage of the VS protocol, we used the bound peptide structure as a query to search collections of small molecules for "hits" that exhibited 3D shapes similar to the octapeptide (H)AVKAASLGK(OH) in Figure 2. To limit the number of structures, we evaluated the multiconformational states of each potential inhibitor from the GRI/NCI database using the ligand shape-based similarity screening technique in the SABRE program. In recent reports, we described the high efficiency of the SABRE algorithm to identify active ligands at different stages (0.1% to 10%) of the screened DUD databases.[43,44]

We docked approximately the top 10% of the active ligands into the $MycP_1$ active site using the fast-and-rigid-docking method of the SABRE program. All active ligands that passed the receptor-shape-fitting filter were scored. Visual inspection of the top 1000 structures (top ~0.3% of the database) served to exclude "false positives" resulting from protein side-chain distortion and/or erroneous ligand binding that overestimated the scoring value of an active ligand with the receptor site. As a consequence, we selected molecular structures that fit into the binding pocket (*i.e.*, had shape complementarity to the octapeptide substrate) and that adopted a conformation similar to the octapeptide backbone in the active site of $MycP_1$.

On the basis of these docking calculations, we tested 81 compounds (15 from NCI and 66 from GRI databases) for their inhibitory activity against the recombinant $MycP_1$. The *in vitro* assays were performed with a single concentration (150 $\mu$M), and these assays disclosed a series of compounds with ~10% to 60% inhibitory activity against $MycP_1$. Finally, we selected two of the best inhibitors, namely compounds **1** and **2** (2.5% of the hits; Figure 3), which inhibited more than 40% of

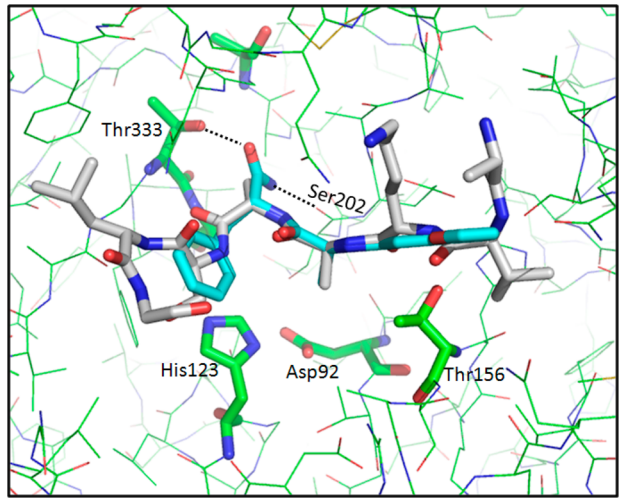


**Figure 3.** Binding mode of compound **1** (NSC-334943) in the $MycP_1$ active site. For comparison, the docked peptide is represented in gray.

the $MycP_1$ activity (Table 1). In comparing the binding of compounds **1** and **2** to (H)AVKAASLGK(OH), we noted that the octapeptide exploited the entire $MycP_1$ binding site, including a deep pocket containing subsite S1 into which the side-chain of (H)AVKAA$^{358}$SLGK(OH) inserted as well as a long cavity where the backbone of (H)AVKAASLGK(OH) fitted. Compounds **1** and **2** were predicted to use the same deep subsite S1 cavity: the amide moiety in compound **1** was crucial to its binding, and the methyl moiety in compound **2** was crucial to its binding in this deep cavity.

We observed that the compounds **1** and **2** were ranked at positions 296 and 31 of the top 1000 selected ligands of the VS and were ranked at positions 25 and 7 in the list of 81 tested


dx.doi.org/10.1021/ci500025r | J. Chem. Inf. Model. 2014, 54, 1166–1173

**Table 1. Experimentally Determined Inhibitory Activity of the 10 Compounds Selected from the Virtual Screening**

| compound | NSC or UC/GRI | % inhibition at 150 $\mu$M | $IC_{50}$ ($\mu$M)[a] | hits tested | % yield of active compounds |
|---|---|---|---|---|---|
| **1** | NSC-334943 | 61% | 135 | 81 | 2.5% |
| **2** | UC-521228 | 42% | ND | | |
| **3** | NSC-334344 | 67% | 146 | 40 | 10% |
| **4** | NSC-657705 | 43% | ND | | |
| **5** | NSC-112182 | 43% | ND | | |
| **6** | NSC-25812 | 41% | ND | | |
| **7** | NSC-176297 | 56% | ND | 25 | 16% |
| **8** | NSC-106893 | 68% | 95 | | |
| **9** | NSC-97914 | 59% | ND | | |
| **10** | NSC-357905 | 73% | 48 | | |

[a]ND: Not Determined.

structures. These results are encouraging and are in good agreement with our previous studies in which the SABRE program provided high enrichment factors (EF) at $EF^{0.1\%}$ (top 100) and $EF^{1\%}$ (top 1000) after screening a large database (95 000 ligands).[44]

To test whether our iterative VS scheme would successfully identify novel inhibitors, the pharmacophore model was used once again to screen the GRI/NCI database. Our approach is distinct from other VS methods in that it uses a "consensus molecular shape pattern" or what we call "4D fingerprints" of active ligands to search out similar structures.[43,44] A visual depiction of this consensus molecular shape pattern is shown in Figure 4. We recently reported that searches using this consensus molecular shape pattern constituted an effective procedure for searches for active compounds within data sets of varying size and structural diversity.[43,44] Using the consensus molecular shape pattern derived from compounds **1** and **2** avoided the need to screen large databases using several different queries and then to rank the ligands using time-consuming, data-fusion methods that in the past often produced false positives.[35]

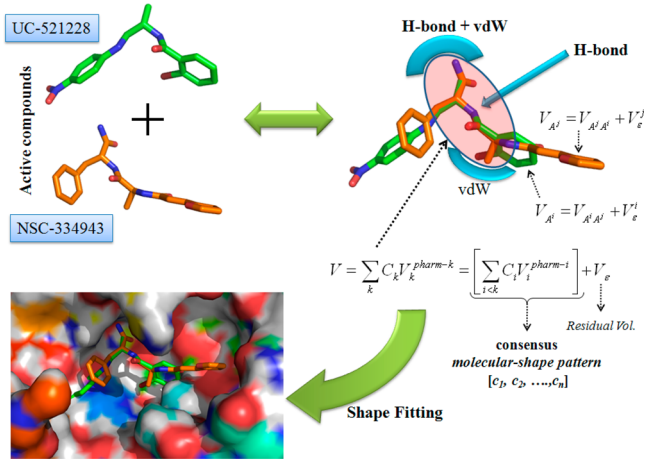


**Figure 4.** Schematic description of the consensus molecular pattern or 4D fingerprint derived from compounds **1** and **2**.

We started the second round of virtual screening of the GRI/NCI database using the structure of compound **1** as a query and the computed 4D fingerprint from compounds **1** and **2**. As before, the top 1000 compounds that resulted from the VS process were selected and visually inspected to eliminate those that did not efficiently span the $MycP_1$ binding site. Forty compounds from the NCI database were then obtained and tested experimentally at a dose of 150 $\mu$M in the high throughput *in vitro* inhibition assay described previously. Four compounds, **3** to **6** (Figure 5; 10% of the hits), showed more

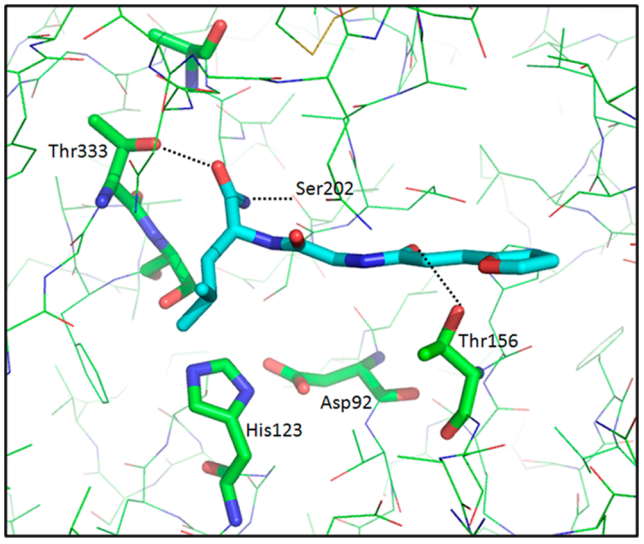


**Figure 5.** Binding mode of compound **3** (NSC-334344) in the $MycP_1$ active site.

than 40% inhibitory activity. At this stage, the query structure **1** permitted the identification of a similar scaffold (compound **3**) to compound **1** as well as highly diverse structural scaffolds (compounds **4**, **5**, and **6**). The resulting "hits" simultaneously served as a means of validating the docking model (since compounds **1** and **3** were similar) and assisted in the identification of new putative compounds for the next iteration of VS. As displayed in Figure 5 and as expected, the amide moiety of compound **3** bound into the S1 site of the $MycP_1$ cavity and formed two H-bonds with Thr333 and Ser202 residues. In addition, the ligand backbone was stabilized in the binding cavity through H-bonding with Thr156 side-chain.

In the next stage of this process, the SABRE program utilized the best structure identified in the previous step, namely compound **3**, as the query, and the 4D fingerprint generated from compounds **1** to **6** for the screening of the GRI/NCI database. From the final top 1000 structures, 25 compounds were assayed for their inhibitory activity against $MycP_1$ protease. As shown in Table 1, four compounds **7**−**10** (Figure 6; 16% of the hits) displayed inhibitory activity of more than 50% at the initial 150 $\mu$M concentration. Although the second-query compound **3** displayed structural similarity to the first-query compound **1**, it permitted the identification of a more diverse subset of compounds than those identified by compound **1**. Thus, the computed 4D fingerprint in the second VS round increased the structural diversity of the scaffolds over those seen in the first VS round (Table 1). The predicted binding conformations of compounds **8** and **10** and


dx.doi.org/10.1021/ci500025r | J. Chem. Inf. Model. 2014, 54, 1166−1173

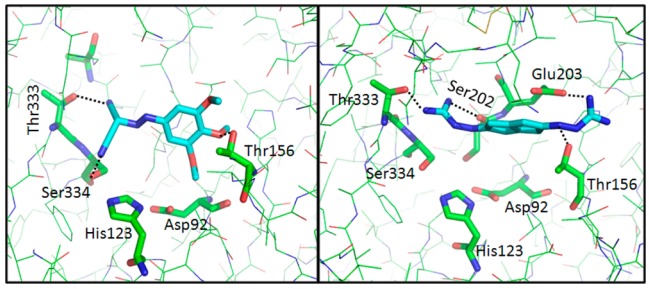


**Figure 6.** Binding mode of compounds **8** (NSC-106893) and **10** (NSC-357905) in the $MycP_1$ active site.

the key interactions with $MycP_1$ are shown in Figure 6. The ligands make van der Waals contacts with the active site and span the S1 subsite, thereby blocking access to the catalytic Ser334−His123−Asp92 triad. Specifically, compound **8** formed hydrogen bonds with the side-chain hydroxyl group of Ser334 and Thr333 in the S1 subsite while the methoxyphenyl moiety of the structure formed hydrogen bonds with the hydroxyl group of the Thr156 side chain and long-range electrostatic interactions with the carboxylate group of the Glu203 residue. Compound **10** interacted mainly via the hydrogen bonds between the primary amino group of the ligand and the Thr333, Ser202, and Thr156 side-chains of $MycP_1$ as well as with long-range electrostatic interactions with the Glu203 side-chain. These interactions are accompanied by van der Waals interactions between the scaffold of the ligand and the Thr156 side-chain. It is striking that compound **10** displays low scaffold similarity to the reference compounds (query) while maintaining a comparable binding mode with highest affinity to $MycP_1$. A superposition of the putative complex structure of compounds (**1**, **3**, **8**, and **10**) in the $MycP_1$ active site is displayed in Supporting Information Figure 4. Structural scaffolds of $MycP_1$ inhibitors identified during the VS campaign are shown in Figure 7.

To highlight the structural diversity of the lead compounds, a 2D heat map of pairwise MACCS fingerprints among the 10 compounds was calculated using the babel program (Figure 8).[51] The 2D heat map shows that most of the compounds have a pairwise similarity ranging from 0.2 to 0.6 (red and green colors), which indicates high structural diversity between the 10 lead compounds. It is interesting to note that the pairwise similarities decrease going from compound 1 to 10 (the pairwise values are reported in Supporting Information Table 2) suggesting the evolution of increasing structural diversity in each VS round.

In summary, the application of the consensus molecular shape pattern-based virtual screening approach, using the SABRE program, identified diverse structural lead compounds for inhibition of $MycP_1$ protease. This study validated the SABRE 4D fingerprint algorithm as a means of enriching compound libraries for active compounds during the VS campaign. The ligand- and structure-based virtual screening approach allowed the utilization of relatively small compound libraries while still discovering a number of interesting lead compounds. These small libraries coupled with the high throughput nature of the *in vitro* screening assay allowed

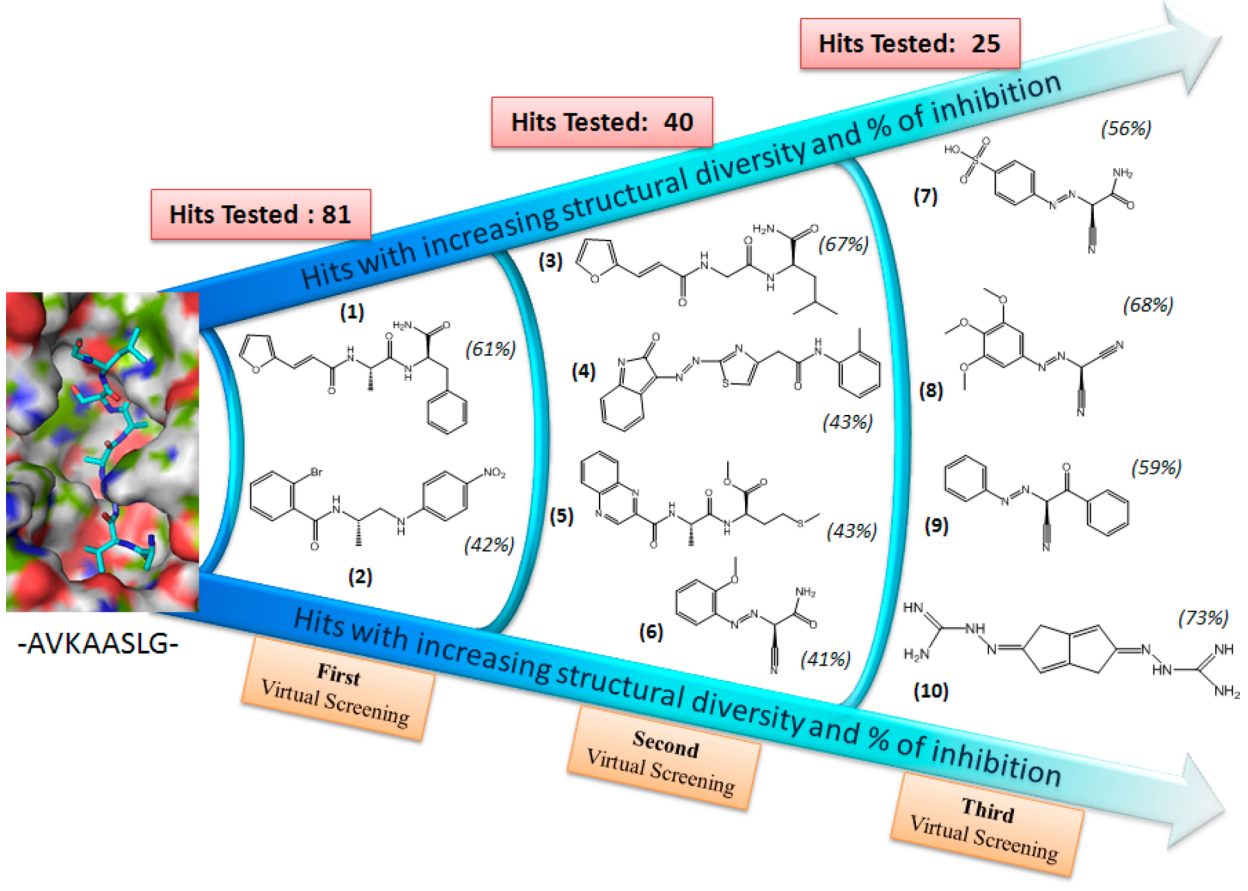


**Figure 7.** Structural scaffolds of $MycP_1$ inhibitors identified during the VS campaign.


dx.doi.org/10.1021/ci500025r | J. Chem. Inf. Model. 2014, 54, 1166−1173

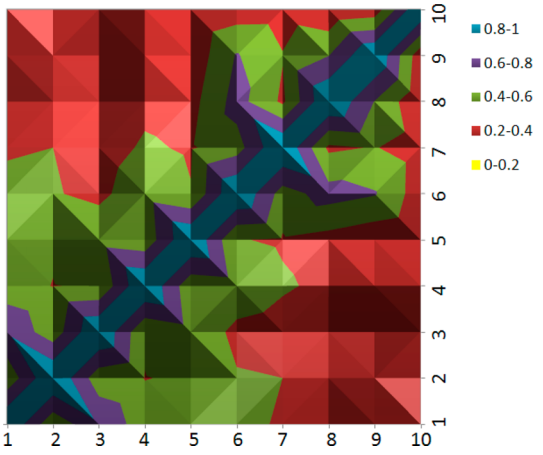


**Figure 8.** 2D heat map of pairwise MACCS fingerprints among the 10 lead compounds.

quick and efficient discovery of novel active scaffolds. These initial scaffolds should prove useful for the development of additional, more potent $MycP_1$ antagonists than those discussed here in a drug discovery process that is now underway. Furthermore, the screening approach described here can be applied for the identification of novel inhibitors to many other proteins of known structure.

## ■ ASSOCIATED CONTENT

### Supporting Information

Computational procedures for the MD simulations and additional Figures and Tables are available free of charge via the Internet at http://pubs.acs.org.

## ■ AUTHOR INFORMATION

### Corresponding Author

*Phone: 859-323-5493. Fax: 859-323-5504. E-mail: kkorotkov@uky.edu.

### Notes

The authors declare no competing financial interest.

## ■ ACKNOWLEDGMENTS

The authors thank Professors Jürgen Bosch at the Johns Hopkins University and Jon Thorson at the University of Kentucky for valuable discussions. We acknowledge the Drug Synthesis and Chemistry Branch of National Cancer Institute for supplying most of the compounds used in the virtual screening and testing. We thank the University of Kentucky Information Technology department and Center for Computational Sciences for computing time on the Lipscomb High Performance Computing Cluster. We acknowledge the University of Kentucky Organic Synthesis Core that is partially supported by grant P20GM103486 from the National Institute of General Medical Sciences (to D.S.W.). This study was supported by NIH/NIGMS grant P20GM103486 (to K.V.K.), and its contents are solely the responsibility of the authors and do not necessarily represent the official views of the NIH or the NIGMS.

## ■ REFERENCES

(1) WorldHealthOrganization. WHO Global tuberculosis report, 2013. http://www.who.int/tb/publications/global_report/en/.

(2) Mdluli, K.; Spigelman, M. Novel targets for tuberculosis drug discovery. *Curr. Opin. Pharmacol.* **2006**, *6*, 459−467.

(3) Koul, A.; Arnoult, E.; Lounis, N.; Guillemont, J.; Andries, K. The challenge of new drug discovery for tuberculosis. *Nature* **2011**, *469*, 483−490.

(4) Arcus, V. L.; Lott, J. S.; Johnston, J. M.; Baker, E. N. The potential impact of structural genomics on tuberculosis drug discovery. *Drug Discovery Today* **2006**, *11*, 28−34.

(5) Zhao, Q. J.; Xie, J. P. *Mycobacterium tuberculosis* proteases and implications for new antibiotics against tuberculosis. *Crit. Rev. Eukaryot. Gene Expr.* **2011**, *21*, 347−361.

(6) Bottai, D.; Serafini, A.; Cascioferro, A.; Brosch, R.; Manganelli, R. Targeting type VII/ESX secretion systems for development of novel antimycobacterial drugs. *Curr. Pharm. Des.* **2013**, DOI: 10.2174/13816128196661311181707l7.

(7) Simeone, R.; Bottai, D.; Brosch, R. ESX/type VII secretion systems and their role in host-pathogen interaction. *Curr. Opin. Microbiol.* **2009**, *12*, 4−10.

(8) Stoop, E. J.; Bitter, W.; van der Sar, A. M. Tubercle bacilli rely on a type VII army for pathogenicity. *Trends Microbiol.* **2012**, *20*, 477−484.

(9) Houben, E. N.; Korotkov, K. V. Bitter, W. Take five — Type VII secretion systems of *Mycobacteria*. *Biochim. Biophys. Acta* **2013**, DOI: 10.1016/j.bbamcr.2013.11.003.

(10) Brown, G. D.; Dave, J. A.; Gey van Pittius, N. C.; Stevens, L.; Ehlers, M. R.; Beyers, A. D. The mycosins of *Mycobacterium tuberculosis* H37Rv: a family of subtilisin-like serine proteases. *Gene* **2000**, *254*, 147−155.

(11) Dave, J. A.; Gey van Pittius, N. C.; Beyers, A. D.; Ehlers, M. R.; Brown, G. D. Mycosin-1, a subtilisin-like serine protease of *Mycobacterium tuberculosis*, is cell wall-associated and expressed during infection of macrophages. *BMC Microbiol.* **2002**, *2*, 30.

(12) Wagner, J. M.; Evans, T. J.; Chen, J.; Zhu, H.; Houben, E. N. G.; Bitter, W.; Korotkov, K. V. Understanding specificity of the mycosin proteases in ESX/type VII secretion by structural and functional analysis. *J. Struct. Biol.* **2013**, *184*, 115−128.

(13) Solomonson, M.; Huesgen, P. F.; Wasney, G. A.; Watanabe, N.; Gruninger, R. J.; Prehna, G.; Overall, C. M.; Strynadka, N. C. Structure of the mycosin-1 protease from the *Mycobacterial* ESX-1 protein type VII secretion system. *J. Biol. Chem.* **2013**, *288*, 17782−17790.

(14) Sun, D.; Liu, Q.; He, Y.; Wang, C.; Wu, F.; Tian, C.; Zang, J. The putative propeptide of MycP1 in mycobacterial type VII secretion system does not inhibit protease activity but improves protein stability. *Protein Cell* **2013**, *4*, 921−931.

(15) McLaughlin, B.; Chon, J. S.; MacGurn, J. A.; Carlsson, F.; Cheng, T. L.; Cox, J. S.; Brown, E. J. A *Mycobacterium* ESX-1-secreted virulence factor with unique requirements for export. *PLoS Pathog.* **2007**, *3*, e105.

(16) Xu, J.; Laine, O.; Masciocchi, M.; Manoranjan, J.; Smith, J.; Du, S. J.; Edwards, N.; Zhu, X.; Fenselau, C.; Gao, L. Y. A unique *Mycobacterium* ESX-1 protein co-secretes with CFP-10/ESAT-6 and is necessary for inhibiting phagosome maturation. *Mol. Microbiol.* **2007**, *66*, 787−800.

(17) Ohol, Y. M.; Goetz, D. H.; Chan, K.; Shiloh, M. U.; Craik, C. S.; Cox, J. S. *Mycobacterium tuberculosis* MycP1 protease plays a dual role in regulation of ESX-1 secretion and virulence. *Cell Host Microbe* **2010**, *7*, 210−220.

(18) Chen, J. M.; Zhang, M.; Rybniker, J.; Boy-Rottger, S.; Dhar, N.; Pojer, F.; Cole, S. T. *Mycobacterium tuberculosis* EspB binds phospholipids and mediates EsxA-independent virulence. *Mol. Microbiol.* **2013**, *89*, 1154−1166.

(19) Chen, J. M.; Pojer, F.; Blasco, B.; Cole, S. T. Towards anti-virulence drugs targeting ESX-1 mediated pathogenesis of *Mycobacterium tuberculosis*. *Drug Discovery Today: Dis. Mech.* **2010**, *7*, e25−e31.

(20) Roberts, D. M.; Personne, Y.; Ollinger, J.; Parish, T. Proteases in *Mycobacterium tuberculosis* pathogenesis: potential as drug targets. *Future Microbiol.* **2013**, *8*, 621−631.

(21) McPhalen, C. A.; James, M. N. Structural comparison of two serine proteinase-protein inhibitor complexes: eglin-c-subtilisin Carlsberg and CI-2-subtilisin Novo. *Biochemistry* **1988**, *27*, 6582−6598.

(22) Kitchen, D. B.; Decornez, H.; Furr, J. R.; Bajorath, J. Docking and scoring in virtual screening for drug discovery: methods and applications. *Nat. Rev. Drug Discovery* **2004**, *3*, 935−949.
(23) Rester, U. From virtuality to reality — Virtual screening in lead discovery and lead optimization: a medicinal chemistry perspective. *Curr. Opin. Drug Discovery Dev.* **2008**, *11*, 559−568.
(24) Kolb, P.; Ferreira, R. S.; Irwin, J. J.; Shoichet, B. K. Docking and chemoinformatic screens for new ligands and targets. *Curr. Opin. Biotechnol.* **2009**, *20*, 429−436.
(25) Kolb, P.; Irwin, J. J. Docking screens: right for the right reasons? *Curr. Top. Med. Chem.* **2009**, *9*, 755−770.
(26) Brooks, W. H.; McCloskey, D. E.; Daniel, K. G.; Ealick, S. E.; Secrist, J. A., 3rd; Waud, W. R.; Pegg, A. E.; Guida, W. C. *In silico* chemical library screening and experimental validation of a novel 9-aminoacridine based lead-inhibitor of human S-adenosylmethionine decarboxylase. *J. Chem. Inf. Model.* **2007**, *47*, 1897−1905.
(27) Hamza, A.; Zhao, X.; Tong, M.; Tai, H. H.; Zhan, C. G. Novel human mPGES-1 inhibitors identified through structure-based virtual screening. *Bioorg. Med. Chem.* **2011**, *19*, 6077−6086.
(28) Yang, W.; AbdulHameed, M. D.; Hamza, A.; Zhan, C. G. New inhibitor of 3-phosphoinositide dependent protein kinase-1 identified from virtual screening. *Bioorg. Med. Chem. Lett.* **2012**, *22*, 1629−1632.
(29) Sorna, V.; Theisen, E. R.; Stephens, B.; Warner, S. L.; Bearss, D. J.; Vankayalapati, H.; Sharma, S. High-throughput virtual screening identifies novel N′-(1-phenylethylidene)-benzohydrazides as potent, specific, and reversible LSD1 inhibitors. *J. Med. Chem.* **2013**, *56*, 9496−9508.
(30) Taylor, R. D.; Jewsbury, P. J.; Essex, J. W. A review of protein-small molecule docking methods. *J. Comput.-Aided Mol. Des.* **2002**, *16*, 151−166.
(31) Coupez, B.; Lewis, R. A. Docking and scoring — theoretically easy, practically impossible? *Curr. Med. Chem.* **2006**, *13*, 2995−3003.
(32) Leach, A. R.; Shoichet, B. K.; Peishoff, C. E. Prediction of protein-ligand interactions. Docking and scoring: successes and gaps. *J. Med. Chem.* **2006**, *49*, 5851−5855.
(33) Reddy, A. S.; Pati, S. P.; Kumar, P. P.; Pradeep, H. N.; Sastry, G. N. Virtual screening in drug discovery — a computational perspective. *Curr. Protein Pept. Sci.* **2007**, *8*, 329−351.
(34) Vainio, M. J.; Puranen, J. S.; Johnson, M. S. ShaEP: molecular overlay based on shape and electrostatic potential. *J. Chem. Inf. Model.* **2009**, *49*, 492−502.
(35) Svensson, F.; Karlen, A.; Skold, C. Virtual screening data fusion using both structure- and ligand-based methods. *J. Chem. Inf. Model.* **2012**, *52*, 225−232.
(36) Yan, X.; Li, J.; Liu, Z.; Zheng, M.; Ge, H.; Xu, J. Enhancing molecular shape comparison by weighted Gaussian functions. *J. Chem. Inf. Model.* **2013**, *53*, 1967−1978.
(37) Hamza, A.; Wei, N. N.; Zhan, C. G. Ligand-based virtual screening approach using a new scoring function. *J. Chem. Inf. Model.* **2012**, *52*, 963−974.
(38) Zhou, M.; Hou, Y.; Hamza, A.; Pain, C.; Zhan, C. G.; Bugni, T. S.; Thorson, J. S. Probing the regiospecificity of enzyme-catalyzed steroid glycosylation. *Org. Lett.* **2012**, *14*, 5424−5427.
(39) Stambouli, N.; Wei, N. N.; Jlizi, A.; Aissa, S.; Abdelmalek, R.; Kilani, B.; Slim, A.; Tiouiri, B. A.; Dridi, M.; Hamza, A.; Ben Ammar Elgaied, A. Structural insight into a novel human CCR5-V130I variant associated with resistance to HIV-1 infection. *J. Biomol. Struct. Dyn.* **2013**, DOI: 10.1080/07391102.2013.819297.
(40) Stambouli, N.; Dridi, M.; Wei, N. N.; Jlizi, A.; Bouraoui, A.; Elgaaied, A. B. Structural insight into the binding complex: beta-arrestin/CCR5 complex. *J. Biomol. Struct. Dyn.* **2014**, *32*, 866−875.
(41) Zhang, W.; Sviripa, V.; Chen, X.; Shi, J.; Yu, T.; Hamza, A.; Ward, N. D.; Kril, L. M.; Vander Kooi, C. W.; Zhan, C. G.; Evers, B. M.; Watt, D. S.; Liu, C. Fluorinated N,N-dialkylaminostilbenes repress colon cancer by targeting methionine S-adenosyltransferase 2A. *ACS Chem. Biol.* **2013**, *8*, 796−803.
(42) Zhou, M.; Hamza, A.; Zhan, C. G.; Thorson, J. S. Assessing the regioselectivity of OleD-catalyzed glycosylation with a diverse set of acceptors. *J. Nat. Prod.* **2013**, *76*, 279−286.
(43) Hamza, A.; Wei, N. N.; Hao, C.; Xiu, Z. L.; Zhan, C. G. A novel and efficient ligand-based virtual screening approach using the HWZ scoring function and an enhanced shape-density model. *J. Biomol. Struct. Dyn.* **2013**, *31*, 1236−1250.
(44) Wei, N. N.; Hamza, A. SABRE: ligand/structure-based virtual screening approach using consensus molecular-shape pattern recognition. *J. Chem. Inf. Model.* **2014**, *54*, 338−346.
(45) Irwin, J. J.; Shoichet, B. K. ZINC — a free database of commercially available compounds for virtual screening. *J. Chem. Inf. Model.* **2005**, *45*, 177−182.
(46) *OMEGA*, version 2.5.1; OpenEye Scientific Software: Santa Fe, NM. http://www.eyesopen.com.
(47) Hawkins, P. C.; Skillman, A. G.; Warren, G. L.; Ellingson, B. A.; Stahl, M. T. Conformer generation with OMEGA: algorithm and validation using high quality structures from the Protein Databank and Cambridge Structural Database. *J. Chem. Inf. Model.* **2010**, *50*, 572−584.
(48) Hawkins, P. C.; Nicholls, A. Conformer generation with OMEGA: learning from the data set and the analysis of failures. *J. Chem. Inf. Model.* **2012**, *52*, 2919−2936.
(49) Mavridis, L.; Hudson, B. D.; Ritchie, D. W. Toward high throughput 3D virtual screening using spherical harmonic surface representations. *J. Chem. Inf. Model.* **2007**, *47*, 1787−1796.
(50) Dror, O.; Schneidman-Duhovny, D.; Inbar, Y.; Nussinov, R.; Wolfson, H. J. Novel approach for efficient pharmacophore-based virtual screening: method and applications. *J. Chem. Inf. Model.* **2009**, *49*, 2333−2343.
(51) O'Boyle, N. M.; Banck, M.; James, C. A.; Morley, C.; Vandermeersch, T.; Hutchison, G. R. Open Babel: An open chemical toolbox. *J. Cheminf.* **2011**, *3*, 33.